Arabian Journal of Chemistry (2023) **16**, 104768

King Saud University

Arabian Journal of Chemistry

www.ksu.edu.sa
www.sciencedirect.com

ORIGINAL ARTICLE

Sonochemical synthesis and characterization of Ho-Cu-O nanostructures and their application as photocatalyst for degradation of water-soluble organic pollutants under UV light

Seyed Milad Tabatabaeinejad [a], Hossein Safardoust-Hojaghan [b], Mojgan Ghanbari [a], Hasan Sh. Majdi [c], Shuaib M. Abdulnabi [d], Furqan S. Hashim [e], Anmar Ghanim Taki [f], Masoud Salavati-Niasari [a,*]

[a] *Institute of Nano Science and Nano Technology, University of Kashan, Kashan P.O. Box 87317-51167, Iran*
[b] *Young Researchers and Elite Club, Marand Branch, Islamic Azad University, Marand, Iran*
[c] *Department of Chemical Engineering and Petroleum Industries, Al-Mustaqbal University College, Babylon 51001, Iraq*
[d] *Department of Medical Instruments Techniques Engineering, Al-Hadba University College, Iraq*
[e] *Department of Medical Laboratories Technology, AL-Nisour University College, Baghdad, Iraq*
[f] *Department of Radiology & Sonar Techniques, AlNoor University College, Nineveh, Iraq*

Received 8 December 2022; accepted 27 February 2023
Available online 13 March 2023

KEYWORDS

$Ho_2Cu_2O_5/Ho_2O_3$ Nanocomposites;
Nanophotocatalyst;
Nanostructures;
Scavenger;
Water pollutants

Abstract Water pollutants have been a significant concern in recent years. It is essential to use advanced materials that effectively reduce these pollutants. This work introduces $Ho_2Cu_2O_5/Ho_2O_3$ nanocomposites as a novel catalyst for photodegradation of various water-soluble organic pollutants. First, $Ho_2Cu_2O_5/Ho_2O_3$ nanocomposites were prepared via a simple and fast ultrasonic-assisted route. The chemical and morphological features of the as-synthesized sample were determined using VSM, FTIR, XRD, EDS, SEM, and TEM analysis. Also, the optical bandgaps and pore diameter were determined to be 3.1, 3.6 eV, and 12.74 nm via ultraviolet–visible diffuse reflectance spectroscopy and Brunauer-Emmett-Teller (BET) for $Ho_2Cu_2O_5$ and Ho_2O_3, respectively. The findings revealed that the prepared nanocomposite could act as a photocatalyst for removing various organic pollutants from water. 93.01% and 92% of Eriochrome black T (ECBT) and Acid yellow (AY) were degraded under UV irradiation at optimum conditions after 120 min (0.03 g of photocatalyst and 10 ppm of pollutants). The kinetics of the ECBT removal was studied through

* Corresponding author.
E-mail address: salavati@kashanu.ac.ir (M. Salavati-Niasari).
Peer review under responsibility of King Saud University.

Production and hosting by Elsevier

https://doi.org/10.1016/j.arabjc.2023.104768

the Langmuir-Hinshelwood model, and the apparent rate of the pseudo-first-order reaction (k = 0.03465 min^{-1}) was obtained. The use of different scavengers made it clear that formation $\bullet O_2^-$ species were primarily responsible for the photodegradation of pollutants.

1. Introduction

With the improvement of human economic and social conditions, a very high tendency to live in better environmental conditions has arisen. Therefore, in recent years, attention to environmental challenges has increased significantly (Patra Shahi et al., 2021; Gondo 2022; Rathi et al., 2021; Sajjadi et al., 2021; Wang et al., 2022; Abdtawfeeq et al., 2022; Liu et al., 2022). Semiconductor photocatalysis has been known as a promising strategy in cutting-edge environmental remediation applications and in many clean energy technologies during the past few years (Parvizi et al., 2019; Tayebee et al., 2020; Al Alwany et al., 2022). In this interesting field, an efficient, inexpensive, stable, and easily separable semiconductor nanophotocatalyst can be achieved, which is capable of light harvesting from economic points of view (Liu et al., 2022; Tang et al., 2023). Therefore, a great deal of research has been recently focused on the progress of efficient semiconductor materials with unrivaled properties to degrade organic pollutants in water (Chen et al., 2023; Xiao et al., 2023). Photocatalysis, defined as a process by which a solid semiconductor with light absorption destroys organic, pharmaceutical, and petrochemical compounds, is one of the green processes to overcome environmental challenges (Mohd Razali et al., 2021; Shi et al., 2022; Sutar et al., 2022; Xie et al., 2021). The photocatalytic process has substantial advantages, such as good efficiency, using economical and free solar energy (Deng et al., 2019; Liu, Tang, et al., 2021; Moghanlou et al., 2021). Since the beginning of the photocatalytic process, the use of semiconductors as an attractive option for photocatalytic processes has always been considered. Conventional semiconductor photocatalysts often belong to the oxide and metal sulfide categories (Fu et al., 2022; Kar et al., 2021; Khataee et al., 2020; Serpone & Emeline, 2012; Wang et al., 2021; Zhang et al., 2019). The use of nanomaterials in the photocatalytic process has attracted more attention via emerging fields of nanoscience and nanotechnology. This attention is due to the unique properties that result the reduction of particle size in nanomaterials (Abdolmohammad-Zadeh & Zamani-Kalajahi, 2020; Geng et al., 2019; Liu, Cheng, et al., 2021; Wei et al., 2021; Wen et al., 2017; Xu et al., 2021).

Copper oxide nanostructures based on rare earth elements have been produced by various routes and applied in the photocatalytic process due to their unique properties (Mosleh et al., 2018; Raizada et al., 2020; Tobaldi et al., 2019). Size and morphology control in these nanostructures is very important because the photocatalytic properties of these nanostructures depend heavily on the size and morphology of nanostructures. The relationship between properties and morphology emphasizes the importance of the methods of synthesis of these nanoparticles since the applied synthesis method determines the morphological characteristics of the copper oxide nanostructures based on rare earth elements (Duan et al., 2021; Shabani et al., 2016; Zhang et al., 2016). In recent years, rare earth-based nanomaterials have been widely prepared and applied in photocatalytic process. This effect can be made through the formation of rare earth oxides nanocomposites with conventional photocatalysts, or by doping rare earth elements into the structure of metal oxide photocatalysts (Kannan et al., 2020; Sordello et al., 2019; Salavati-Niasari et al., 2009; Bobinov et al., 2021).

Muhammad Rakibul Islam and co-authors prepared copper oxide and cerium-doped copper oxide nanostructures via the sol–gel auto combustion route. In this study, the effect of cerium content was studied on morphological, optical, structural, and electrical properties. Results revealed that the presence of cerium induces intrinsic defects in the cerium-doped copper oxide nanoparticles and changes the optical bandgap from 1.72 eV to 1.40 eV. The photodegradation activity of copper oxide and cerium-doped copper oxide nanoparticles was studied by examining the degradation of methylene blue under visible light irradiation. Cerium-doped copper oxide nanoparticles show superior photocatalytic performance in comparison with copper oxide nanoparticles. It was reported that the narrowing of the bandgap along with the presence of shallow doping states allows sufficient charge separation along with enhanced photon adsorption of cerium-doped copper oxide nanoparticles, leading to an improved photodegradation process (Islam et al., 2021).

In another report, lanthanum-doped $NaTaO_3$ was synthesized via a solution-based route. Then, the prepared lanthanum-doped $NaTaO_3$ was decorated with copper oxide nanoparticles with different concentrations to design new visible-light-induced photocatalysts. Copper oxide/lanthanum-doped $NaTaO_3$ showed mesoporous properties and specific surface areas of 199 to 221 m^2/g in comparison with 230 m^2/g for pristine lanthanum-doped $NaTaO_3$. It was reported that at 3.0 wt% dosage of copper oxide nanoparticles, incorporation of the copper oxide in lanthanum-doped $NaTaO_3$ makes a sample via a wide absorption in the 400–700 nm and a significant reduction of the E_g from 4.05 to 2.1 eV. The study was aimed at photodegradation of ciprofloxacin via as-prepared copper oxide/ lanthanum-doped $NaTaO_3$. After 60 min of visible light irradiation, the 2.0 $g.L^{-1}$ dosage of 3%copper oxide/lanthanum-doped $NaTaO_3$ achieved complete degradation of ciprofloxacin via a photoreaction rate of 0.071 min^{-1} and provided considerable recyclability of 5 cycles. The development of a heterojunction between copper oxide and lanthanum-doped $NaTaO_3$ was credited with copper oxide/lanthanum-doped $NaTaO_3$ photocatalytic activity. Photoluminescence and photocurrent tests indicated that the as-obtained heterojunction enhanced photoinduced charge separation and mobility (Shawky et al., 2021).

This study aimed to introduce a novel and superior photocatalyst, $Ho_2Cu_2O_5/Ho_2O_3$ nanocomposites, for the photodegradation of organic pollutants. For the first time, the $Ho_2Cu_2O_5/Ho_2O_3$ nanocomposites were prepared via a sonochemical route at the different experimental conditions to modify their structural and morphological properties. The properties of as-obtained samples were examined via XRD, FTIR, EDS, SEM, TEM, and UV–Vis (DRS) analysis comprehensively. Optimized $Ho_2Cu_2O_5/Ho_2O_3$ nanocomposites were applied for photodegradation of Eriochrome black T (ECBT), as a common dye-based pollutant.

2. Experimental

2.1. Materials

Copper nitrate trihydrate 99% ($Cu(NO_3)_2{\cdot}3H_2O$), Holmium (III) nitrate pentahydrate 99.9% ($Ho(NO_3)_3{\cdot}5H_2O$), tetraethylenepentamine (TEPA), Ethylenediaminetetraacetic acid (EDTA) benzoic acid (BA), and 4-Benzoquinone (BQ), were procured from Merck Company and applied with no extra purifying.

2.2. Synthesis of $Ho_2Cu_2O_5/Ho_2O_3$ nanocomposites

550 mg (1.25 mmol) of $Ho(NO_3)_3$ was dissolved in distilled water under magnetic stirring. In another container, 300 mg

(1.25 mmol) of $Cu(NO_3)_2$ was dissolved in distilled water under stirring. It should be noted that the molar ratio of Cu to Ho was considered 1:1. The Cu-containing solution was added to the Ho-containing solution. The as-obtained solution was irradiated via ultrasonic (45 W power) at different times. TEPA, a basic agent, was added dropwise to the solution during ultrasonication until pH reached 10. In this step, the solid product was precipitated from the solution. After 30 min, ultrasonication was stopped, and the obtained mixture was transferred to the magnetic stirrer at 80 ℃. After 20 min, the gel-like product was formed. The obtained gel was dried at 70 ℃ for 24 h. Finally, the dried gel was calcined at 700 and 1000 ℃.

2.3. Characterization

XRD patterns were obtained from a Philips-X'pertpro X-ray diffractometer with Ni-filtered Cu K radiation. The surface functional group was investigated via Fourier-transform infrared spectroscopy, which was obtained from a Nicolet Magna-550 spectrometer in KBr pellets. The LEO-1455VP scanning electron microscope, which was fitted with an EDS spectroscopy, was used to examine the shape and size of the samples. The transmission electron microscope images were applied to study the shape and size recorded by Philips EM208 transmission electron microscope. The magnetic characteristics were analyzed via a vibrating sample magnetometer (VSM, Meghnatis Kavir Kashan Co., Kashan, Iran). All chemical analyses were carried out using a GC-2550TG (Teif Gostar Faraz Company, Iran).

2.4. Photocatalytic test

The photocatalytic activity of prepared nanocomposites was comprehensively studied against methyl orange, methyl violet, acid red, eriochrome black T, malachite green, rhodamine B, eosin, acid black, and acid yellow at room temperature. The photocatalytic tests were done as follows: A 10 ppm concentration of the examined dyes was prepared separately. 300 mg of prepared $Ho_2Cu_2O_5/Ho_2O_3$ was dispersed in 50 mL of dye solutions. The mixture was then stirred in the dark for 30 min to complete the adsorption equilibrium of dyes on the surface of the photocatalyst. After that, the xenon arc lamp was turned on to provide UV light to irradiate the as-prepared mixture. After every interval of 15 min, 5 mL of the solution was taken out and centrifuged. The light absorbance of the provided solution was tested by an ultraviolet spectrophotometer, and the dosage of the pollutants within the obtained solution was determined based on the absorbance of light at the maximum wavelength of pollutants.

3. Results and discussion

3.1. Structural and morphological properties of $Ho_2Cu_2O_5$/ Ho_2O_3 nanocomposites

Fig. 1 shows the XRD patterns of samples produced at various calcination temperatures and times. Fig. 1a displays the XRD pattern of the prepared sample after calcination at 700 ℃ for

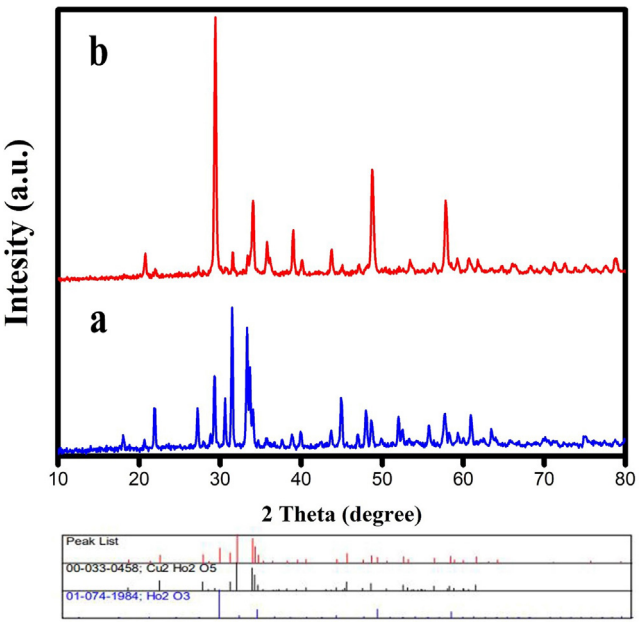

Fig. 1 XRD pattern of prepared samples after calcination at a) 1000 ℃ for 8 h b) 700 ℃ for 4 h.

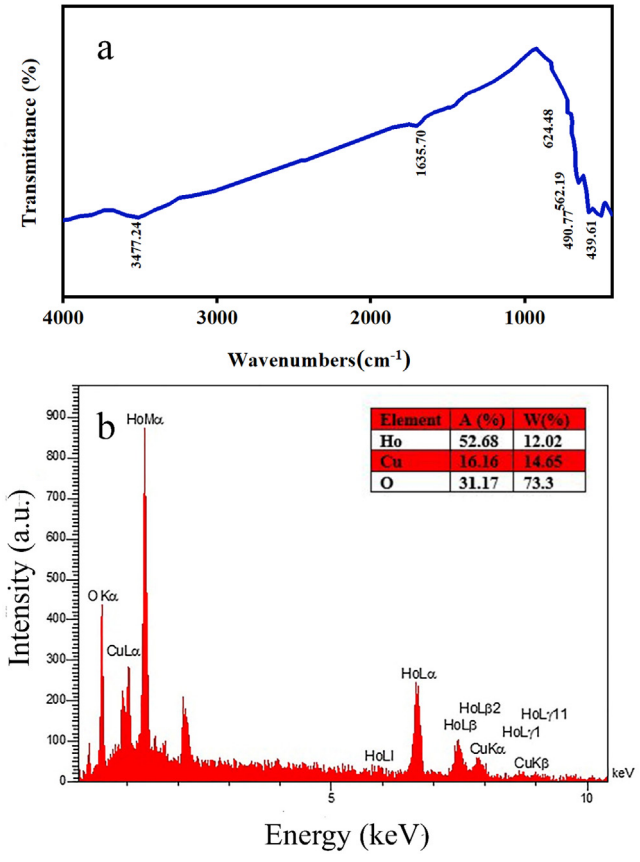

Fig. 2 A) ftir spectrum, and b) eds analysis of synthesized ho_2-Cu_2O_5/Ho_2O_3 nanocomposites prepared with a power of 45 W for 10 min and 0.5 s pulse rate.

4 h, and Fig. 1b is related to the product after calcination at 1000 ℃ for 8 h. The temperature and time of calcination affect the structural properties of samples substantially. It is found that pure $Ho_2Cu_2O_5/Ho_2O_3$ nanocomposites are not formed after 4 h of calcination at 700 ℃. In Fig. 1a, the $Ho_2Cu_2O_5$-related peaks are not observed and the Ho_2O_3-related peaks are prominent. The $Ho_2Cu_2O_5/Ho_2O_3$ nanocomposites are formed without any impurities by increasing calcination time and temperature. This can be due to the low activation energy at low temperatures that do not allow $Ho_2Cu_2O_5$ formation. The same result was reported previously via Rui Guo et al (Guo et al., 2017). They found that at a calcination temperature of below 800 ℃, no $Ho_2Cu_2O_5$ was formed. Fig. 1b shows the formation of the orthorhombic structure of $Ho_2Cu_2O_5$

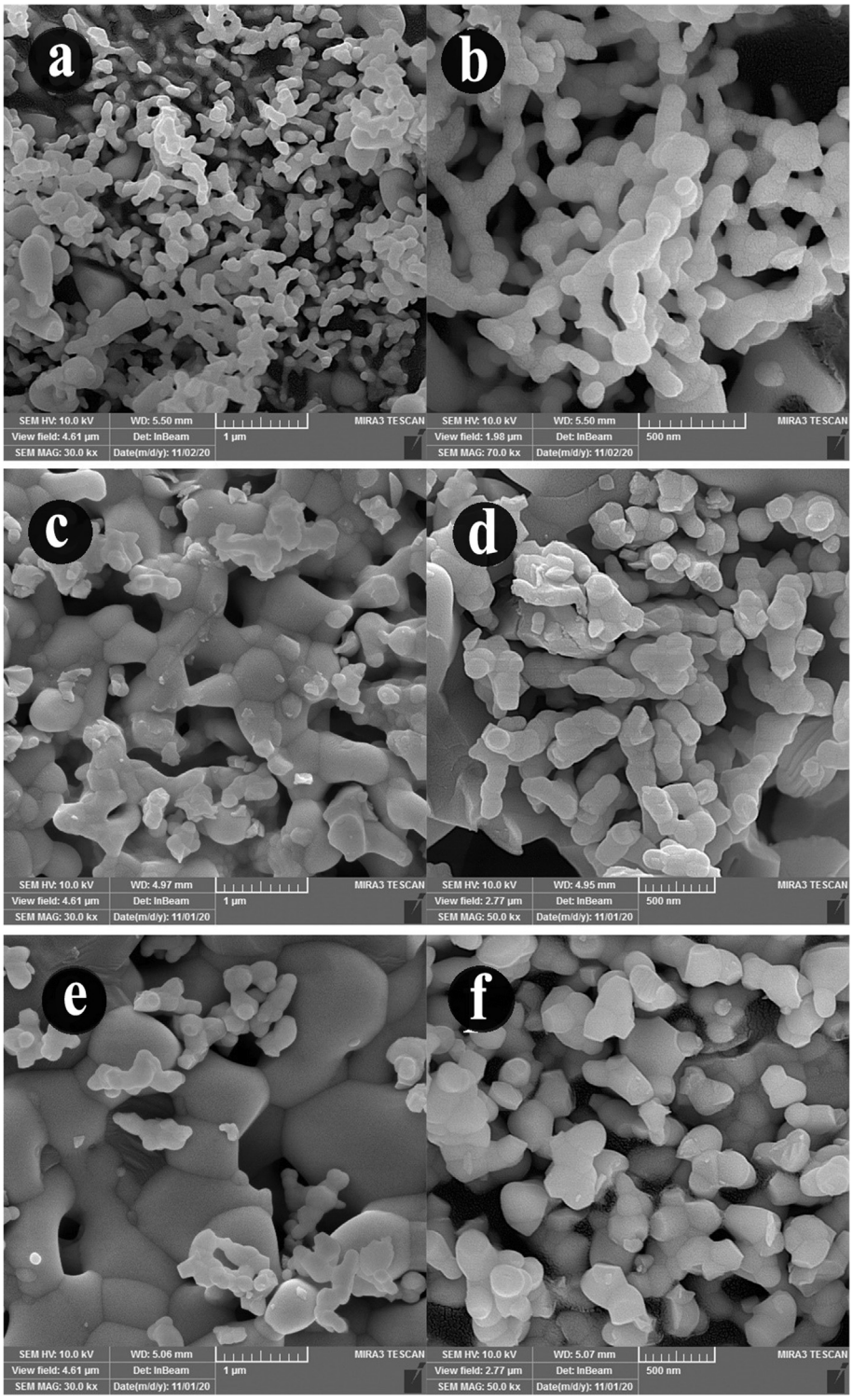

Fig. 3 The SEM images of $Ho_2Cu_2O_5/Ho_2O_3$ nanocomposites prepared with a power of 45 W for a,b) 10 min c,d) 20, and e,f) 30 min.

with JCPDS No. 00–033-0458. Also, the Ho_2O_3 has a cubic structure with JCPDS no: 01–074-1984. The width of the obtained XRD peaks leads to small grain size. Based on the XRD results, 8 h calcination at 1000 ℃ is considered an optimum calcination condition. FTIR analysis was applied for further investigation of the structural properties of the prepared $Ho_2Cu_2O_5/Ho_2O_3$ nanocomposites. Fig. 2a shows the FTIR spectrum of $Ho_2Cu_2O_5/Ho_2O_3$ nanocomposites. The presence of a broad peak at 3471 cm^{-1} is related to the stretching band of hydrogen bonds on the surface of the prepared sample (O–H) (Salavati-Niasari, 2005). The peaks at 490 and 562 cm^{-1} are related to the holmium-oxygen (Ho-O) bond. The two mild bands at 439.61 cm^{-1} and 624.48 cm^{-1} may be related to the A_u and B_u modes of the copper-oxygen (Cu–O) bond (Tabatabaeinejad, Amiri, et al., 2021), respectively. It can be concluded from FTIR that $Ho_2Cu_2O_5/Ho_2O_3$ nanocomposites are formed purely and no by-product-related stretching modes are observed. EDS analysis is applied to determine the chemical composition of the prepared sample. The results confirm the presence of holmium, copper, and oxygen elements which confirms the formation of oxides of Cu and Ho (Fig. 2b).

Sonochemical-assisted synthesis is a fast and simple route used in the preparation of nanostructures. Here, the effect of time and power of ultrasonic irradiation was investigated on the morphological properties of $Ho_2Cu_2O_5/Ho_2O_3$ nanocomposites via scanning electron microscopy (SEM). Fig. 3(a-f) shows the SEM images of as-obtained $Ho_2Cu_2O_5/Ho_2O_3$ nanocomposites under different time of ultrasonic irradiation (10, 20, and 30 min). Two different magnifications of SEM images are provided for a better investigation of morphological features. SEM images confirm that the optimum time for $Ho_2Cu_2O_5/Ho_2O_3$ preparation with desirable morphological properties is 10 min. As shown, at 10 min, the porous network, including tiny nanoparticles, is formed (Fig. 3(a-b)), while the irregular larger particles are formed via increasing sonication time for 20 and 30 min. Also, the prepared nanoparticles after 20 min (Fig. 3(c-d)) sonication have lower particle sizes than those prepared at 30 min (Fig. 3(e-f)) sonication. The very tiny particles with higher surface energy are formed via increasing the sonication time, which facilitates the particle agglomeration process. The result of this process is the formation of non-uniform morphology and a larger particle size. Similar results have already been reported confirming these results (Hujjatul Islam et al., 2019; Salavati-Niasari., 2004). Fig. 4(-a-d) provides SEM images of prepared products after 10 min at two different sonication time pulses (0.1 s and 0.5 s). It can be concluded that the applied pulsed ultrasonic affects the size and morphology of prepared $Ho_2Cu_2O_5/Ho_2O_3$

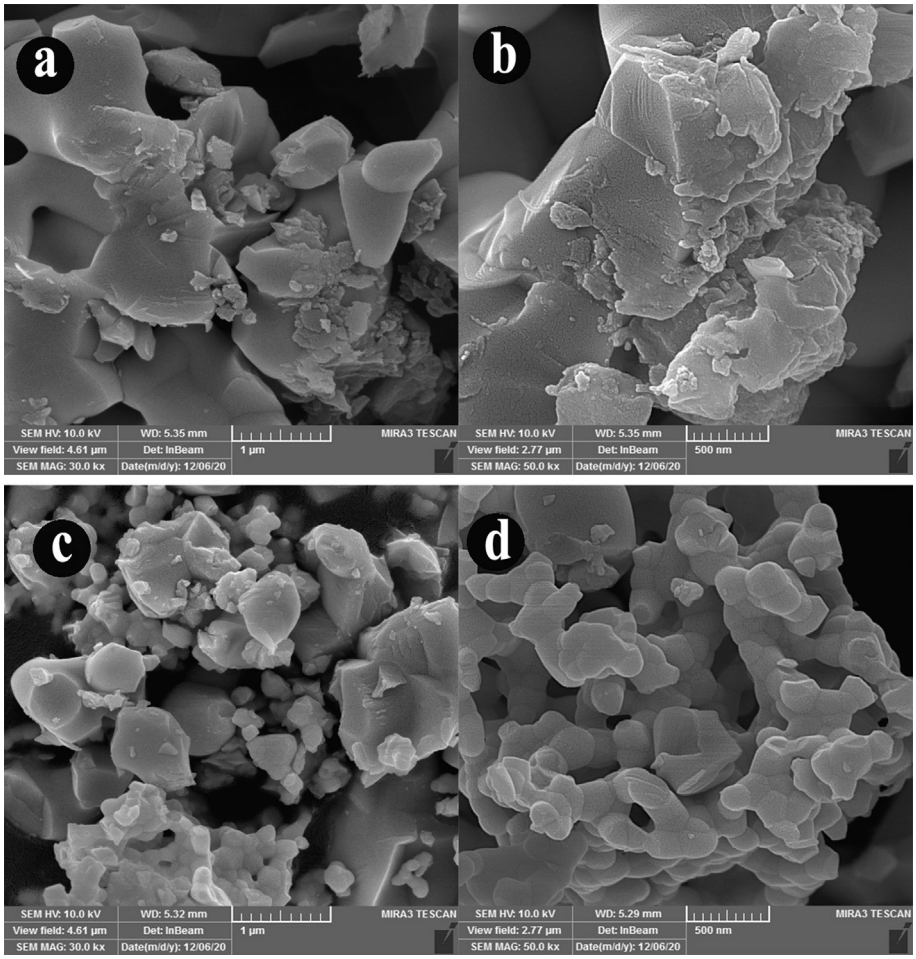

Fig. 4 The SEM images of $Ho_2Cu_2O_5/Ho_2O_3$ nanocomposites prepared with a power of 45 W for 10 min at sonication time pulse a,b) 0.1 s and c,d) 0.5 s.

nanocomposites. It is found that the 0.5 s pulse rate (Fig. 4(c-d)) provides uniform morphology with a smaller particle size than the 0.1 s pulse rate (Fig. 4(a-b)). Transmission electron microscope (TEM) images were applied for further investigation of morphology and particle size. Fig. 5(a-b) shows TEM images of prepared $Ho_2Cu_2O_5/Ho_2O_3$ nanocomposites with a power of 45 W for 10 min, and 0.5 s pulse rate. It can be observed that $Ho_2Cu_2O_5$ particles with a diameter of 30 nm are formed with 35 nm Ho_2O_3 particles as $Ho_2Cu_2O_5/Ho_2O_3$ nanocomposites with uniform morphology.

The surface features of prepared $Ho_2Cu_2O_5/Ho_2O_3$ nanocomposites are determined via nitrogen adsorption/desorption isotherm as well as pore size distribution. The obtained isotherm confirms that the prepared sample belongs to type IV (Fig. 6). The particle size was measured in the range of 1 to 98 nm by applying the BJH route. The BET surface area, pore volume, and pore diameter were calculated at 2.5972 m^2/g, 0.0082733 cm^3/g, and 12.742 nm, respectively. The results prove that the applied ultrasonic-based process provides a sufficient method for the preparation of high-surface-area products.

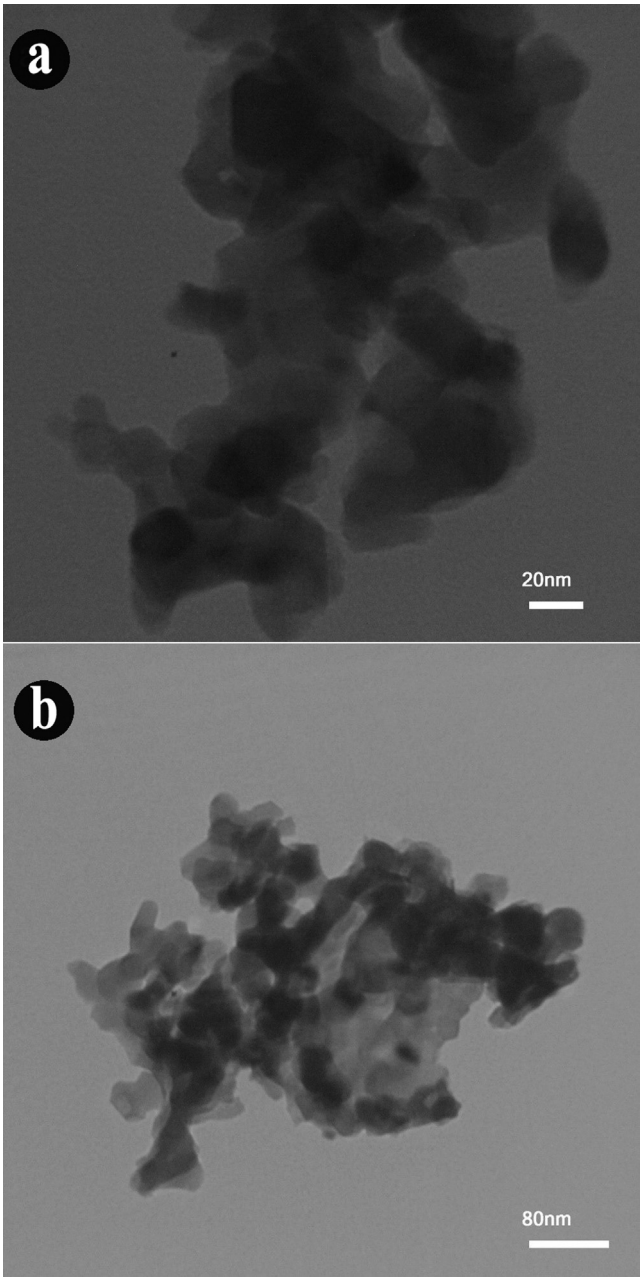

Fig. 5 TEM images of synthesized $Ho_2Cu_2O_5/Ho_2O_3$ nanocomposites prepared with a power of 45 W for 10 min and 0.5 s pulse rate.

VSM analysis was applied for the investigation of the magnetic properties of prepared nanocomposites (Fig. 7). As well as shown, no hysteresis was observed in the B-H graph and the obtained curve is completely reversible. This finding can be justified by the superparamagnetic feature of prepared $Ho_2Cu_2O_5/Ho_2O_3$ nanocomposites. The maximum saturation magnetization (Ms) of the sample is measured at 0.25 emu per gram. This superior magnetic property can be linked to the higher reusability of $Ho_2Cu_2O_5/Ho_2O_3$ nanocomposites in the photocatalytic process.

3.2. Photocatalytic activity of $Ho_2Cu_2O_5/Ho_2O_3$ nanocomposites

The optical properties of nanomaterials are the main determination of photocatalytic properties, so the optical properties of synthesized $Ho_2Cu_2O_5/Ho_2O_3$ nanocomposites were investigated through UV–Vis diffuse reflectance spectroscopy. Fig. 8a shows UV–Vis diffuse reflectance spectroscopy of prepared $Ho_2Cu_2O_5/Ho_2O_3$ nanocomposites with a power of 45 W for 10 min. From it, the Tauc plot was illustrated via the Tauc equation. As seen, the optical band gap is calculated via plotting $(\alpha h\upsilon)^2$ vs $h\upsilon$ (Fig. 8b). According to the prediction, two different band gaps were determined: 3.6 eV for Ho_2O_3 and 3.1 eV for $Ho_2Cu_2O_5$. The measured band gaps provide excellent optical characteristics for the photocatalytic process under UV irradiation. Fig. 9 shows the photocatalytic performance of prepared nanocomposites to the removal of various organic dyes (Methyl orange (MO), Methyl violet (MV), Acid red (AR), Eriochrome black T (ECBT), Malachite green (MG), Rhodamine B (RhB), Eosin (EO), Acid black (AB), and Acid yellow (AY). After 120 min UV illumination, the degradation efficiencies for MO, MV, AR, ECBT, MG, RhB, EO, AB, and AY are measured 40 %, 49.84%, 65.60%, 93.01%, 81.30%, 29%, 89.6.%, 55.93%, and 10.70%, respectively (Fig. 9 (a-b)). The findings show that $Ho_2Cu_2O_5/Ho_2O_3$ nanocomposites had the best photocatalytic performance against ECBT with 93.01% degradation. So, the ECBT was applied for further investigation of the photocatalytic performance of $Ho_2Cu_2O_5/Ho_2O_3$ nanocomposites. The Langmuir-Hinshelwood first-order reaction kinetics model was utilized for in-depth studying of the kinetics of tested dyes removal under ultraviolet irradiation:

$$-\ln(C/C_0) = kt \quad (1).$$

The slope of the plot provided the chemical rate constant, k. The calculated k for all tested dyes is displayed in Fig. 9(-c-d). The maximum k of 0.03465 min^{-1} for ECBT was measured by the pseudo-first-order reaction kinetics equation that shows a higher k in comparison with other tested pollutants.

Fig. 10a shows the effect of dye concentration on the photocatalytic performance of $Ho_2Cu_2O_5/Ho_2O_3$ nanocomposites.

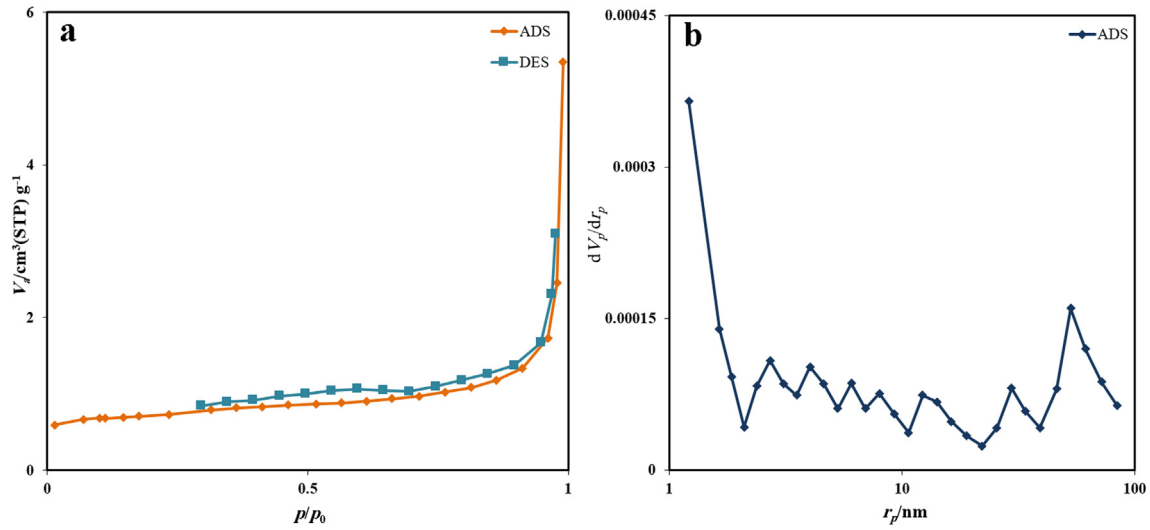

Fig. 6 Nitrogen adsorption–desorption isotherms of $Ho_2Cu_2O_5/Ho_2O_3$ nanocomposites prepared with a power of 45 W for 10 min and 0.5 s pulse rate.

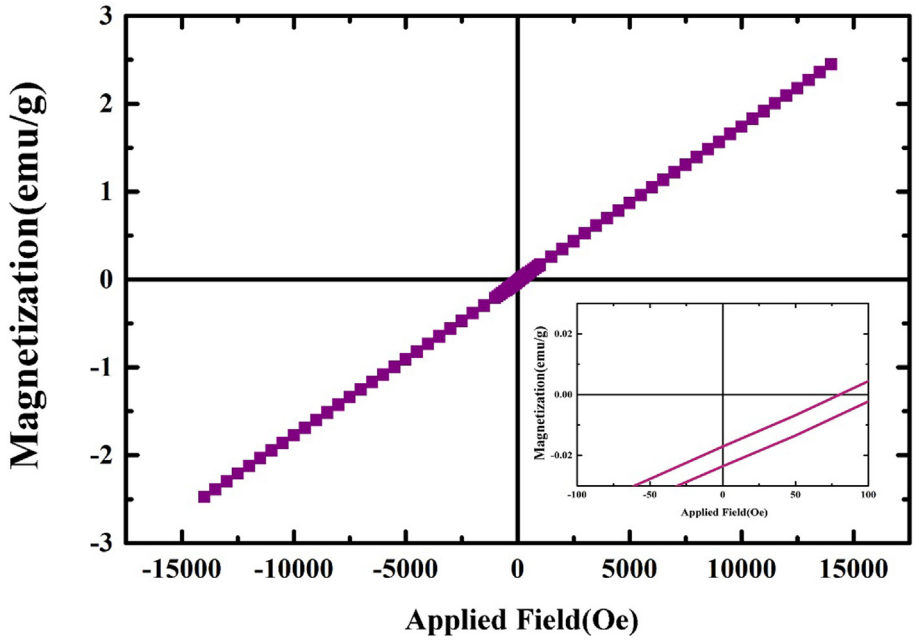

Fig. 7 VSM analysis of prepared $Ho_2Cu_2O_5/Ho_2O_3$ nanocomposites with a power of 45 W for 10 min and 0.5 s pulse rate.

The photocatalytic efficiencies in the 5 ppm (62.5%) and 10 ppm (93.01%) are higher than 15 ppm (22.10%) and 20 ppm (38.53%) of ECBT. The higher photocatalytic activity in the lower dosage of ECBT can be related to the reduction of active sites on the catalyst surface via increasing dye concentration. The ECBT molecules are linked on the surface of $Ho_2Cu_2O_5/Ho_2O_3$ nanocomposites and this leads to disrupting the process of receiving ultraviolet light by the $Ho_2Cu_2O_5/Ho_2O_3$ nanocomposites and finally causes the prevention of hydroxyl radical formation. Also, the adsorbed ECBT molecules on the surface of the catalyst act as a barrier for the reaction between photo-induced holes or radicals and dye molecules. But the results show the higher photocatalytic activity of $Ho_2Cu_2O_5/Ho_2O_3$ nanocomposites against 10 ppm ECBT than 5 ppm ECBT. This may be attributed to the fact that since the initial ECBT dosage increase, more ECBT molecules are available for generation charge carriers, and this lead to a higher probability of hydroxyl radical formation and result in higher photocatalytic efficiency (Reza et al., 2017). Fig. 10b shows the measured k value for photodegradation of different concentrations of ECBT. The photodegradation rate at 10 ppm of ECBT is higher than 5 ppm, 15 ppm, and 20 ppm. Fig. 10c shows the photocatalytic activity of $Ho_2Cu_2O_5/Ho_2O_3$ nanocomposites under ultraviolet and visible light irradiation. According to the results obtained from UV–Vis diffuse reflectance spectroscopy and calculated band gaps, it

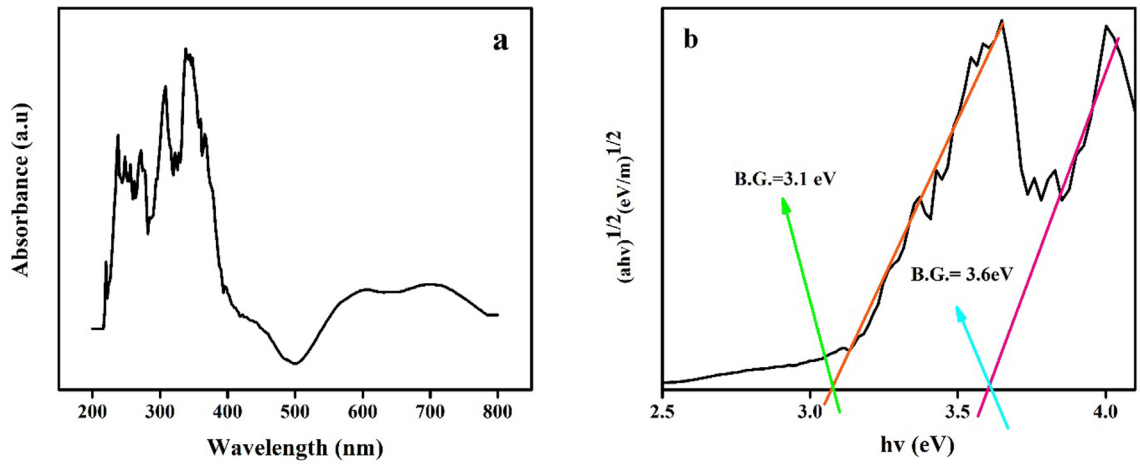

Fig. 8 A) uv–vis diffuse reflectance spectra and b) band gap energies of prepared $Ho_2Cu_2O_5/Ho_2O_3$ nanocomposites with a power of 45 W for 10 min and 0.5 s pulse rate.

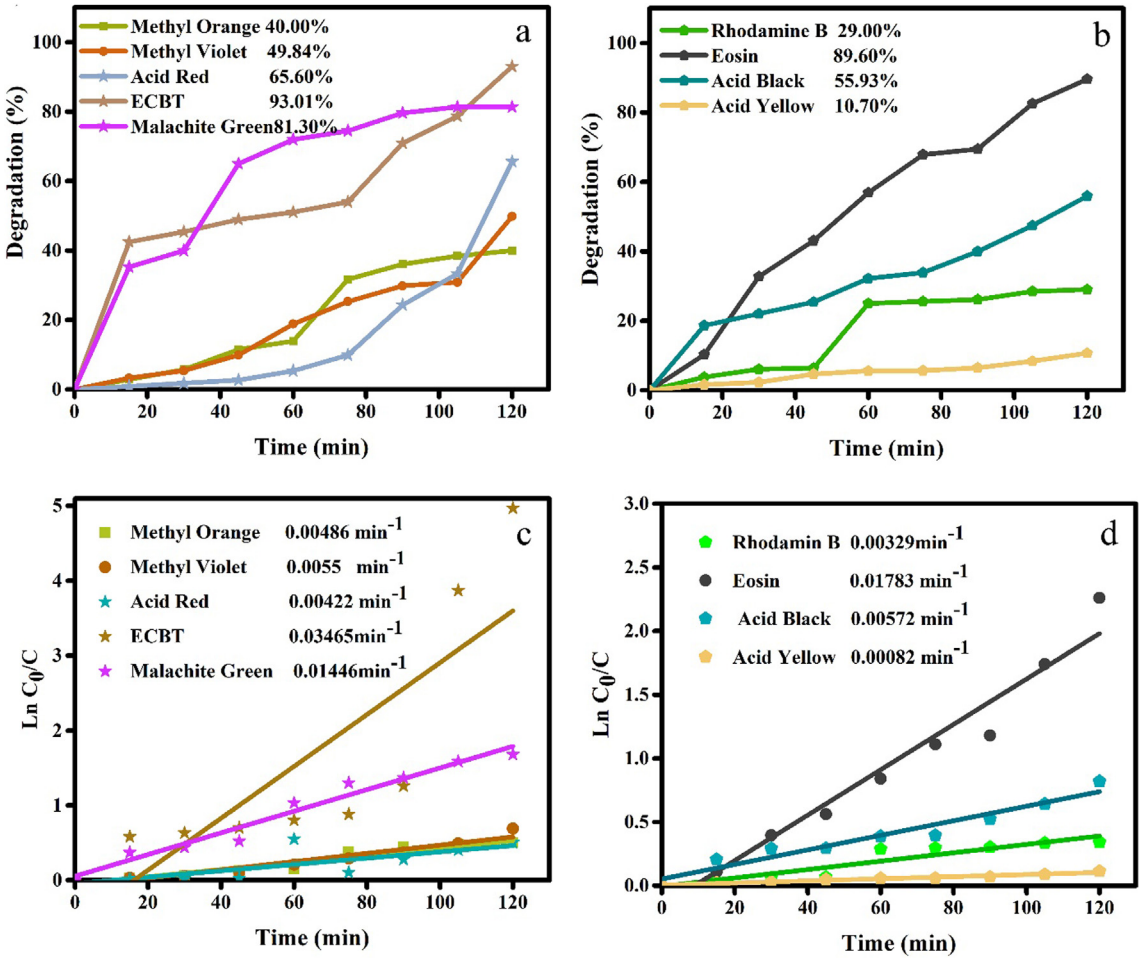

Fig. 9 Photocatalytic activity and kinetic linear simulation plots of $Ho_2Cu_2O_5/Ho_2O_3$ nanocomposites for removal of a,b) Methyl orange (MO), Methyl violet (MV), Acid red (AR), Eriochrome black T (ECBT), Malachite green (MG), c,d) Rhodamine B (RhB), Eosin (EO), Acid black (AB), and Acid yellow (AY) after 120 min UV illumination.

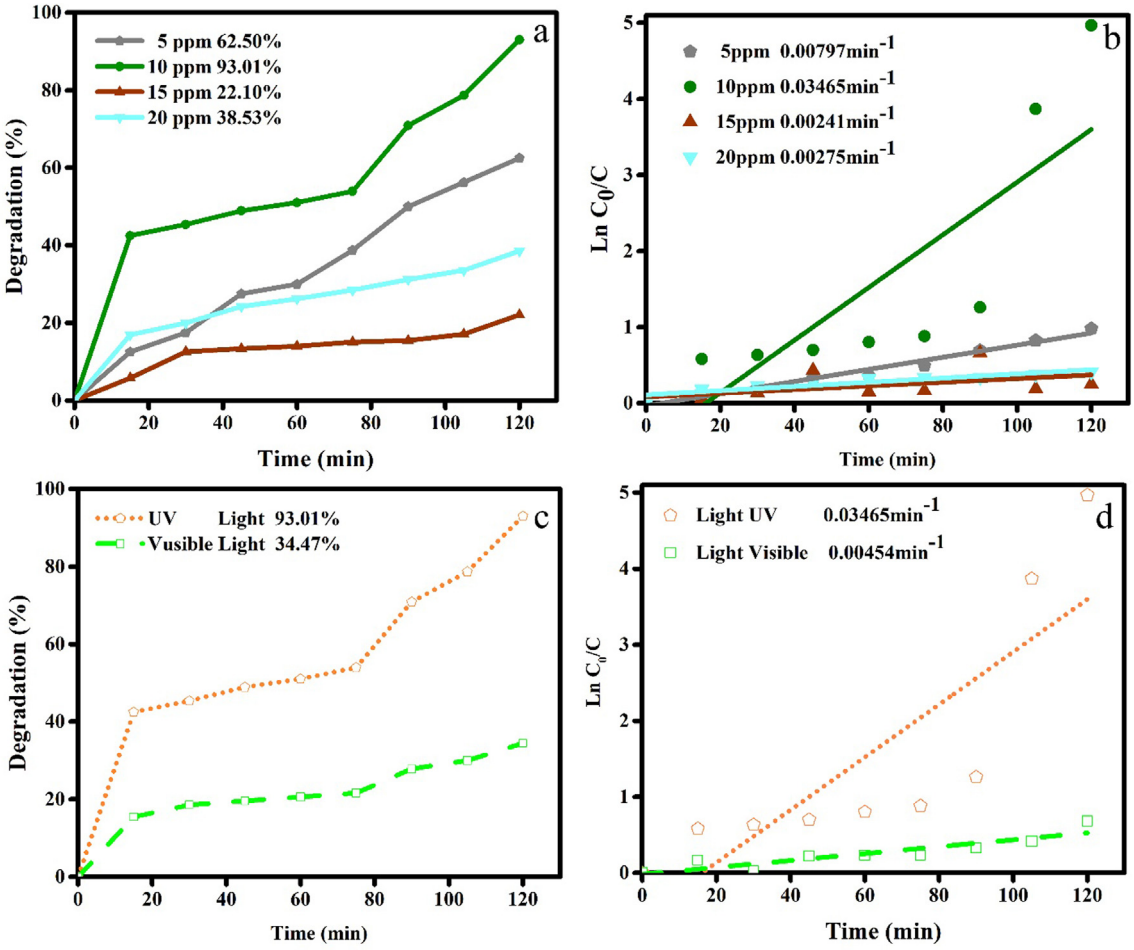

Fig. 10 Photocatalytic performance and kinetic linear simulation plots of $Ho_2Cu_2O_5/Ho_2O_3$ nanocomposites under a, b) different dye concentrations (5, 10, 15, 20 ppm) and c,d) different light sources.

was predictable that the photocatalytic activity of $Ho_2Cu_2O_5/Ho_2O_3$ nanocomposites under ultraviolet light (93.01%) was much higher than the photocatalytic activity under visible light (34.47%). Fig. 10d displays measured k for the photocatalytic process under visible light (0.00454 min^{-1}) and UV irradiation (0.03465 min^{-1}).

3.2.1. Proposed mechanism of $Ho_2Cu_2O_5/Ho_2O_3$ photocatalyst

To understand the mechanism of photodegradation of ECBT via $Ho_2Cu_2O_5/Ho_2O_3$ nanocomposites, ethylenediaminetetraacetic (EDTA), benzoic acid (BA), and benzoquinone (BQ), were used as a scavenger of h^+, •OH, and $•O_2^-$, respectively. As shown in Fig. 11a, BA has a negligible effect on the photocatalytic degradation of ECBT, while BQ causes a significant reduction in photocatalytic efficiency. Fig. 11b shows the obtained results from the kinetic study of ECBT photodegradation via different scavengers. From Fig. 11, it can be concluded that ECBT photodegraded through formation h^+ and $•O_2^-$ species. So, the possible photodegradation mechanism can be described as Eqs. (2)–(8) (Yousefzadeh et al., 2022):

$$Ho_2Cu_2O_5/Ho_2O_3 + h\nu(UV) \rightarrow Ho_2Cu_2O_5/Ho_2O_3\ (e_{CB}^-) + Ho_2Cu_2O_5/Ho_2O_3(h_{VB}^+) \quad (2)$$

$$O_2 + e^- \rightarrow •O_2^- \quad (3)$$

$$•O_2^- + H^+ \rightarrow •HO_2 \quad (4)$$

$$2•HO_2 \rightarrow O_2 + H_2O_2 \quad (5)$$

$$H_2O_2 + e_{CB}^- \rightarrow 2•HO \quad (6)$$

$$h_{VB}^+ + H_2O \rightarrow •HO + 2H^+ \quad (7)$$

$$ECBT + •HO \rightarrow \text{Degradation of ECBT} \quad (8)$$

The proposed mechanism and determined band gap energies show the synergistic interaction between $Ho_2Cu_2O_5$ and Ho_2O_3 that has increased the photocatalytic activity of $Ho_2Cu_2O_5/Ho_2O_3$ nanocomposites against ECBT. The proposed mechanism for photocatalytic degradation of ECBT is provided in Scheme 1.

3.2.2. Recyclability

One of the most influential features of heterogeneous semiconductor photocatalysts is their recyclability, which reduces expenses. Therefore, $Ho_2Cu_2O_5/Ho_2O_3$ nanocomposites were reused five times in the photocatalytic process. Based on

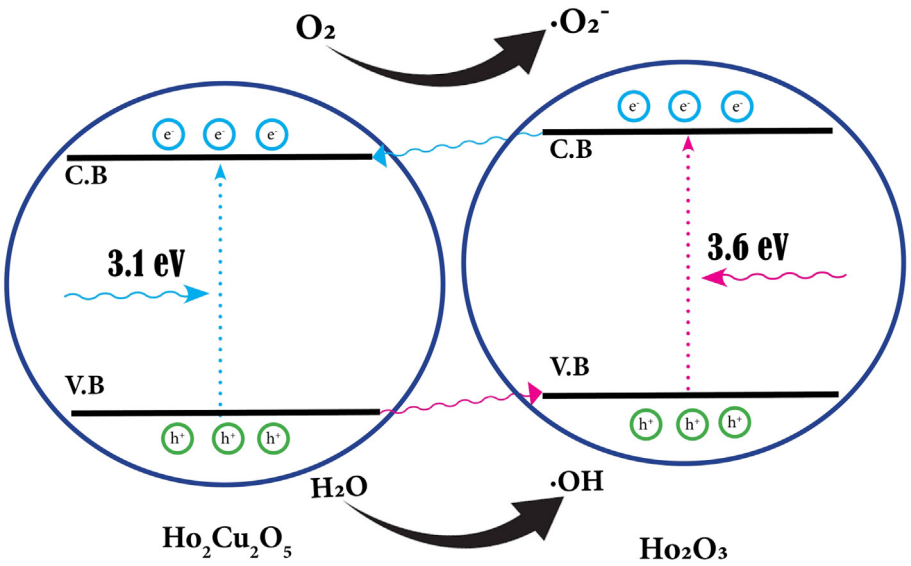

Scheme 1 Photocatalytic degradation mechanism of $Ho_2Cu_2O_5/Ho_2O_3$ nanocomposites.

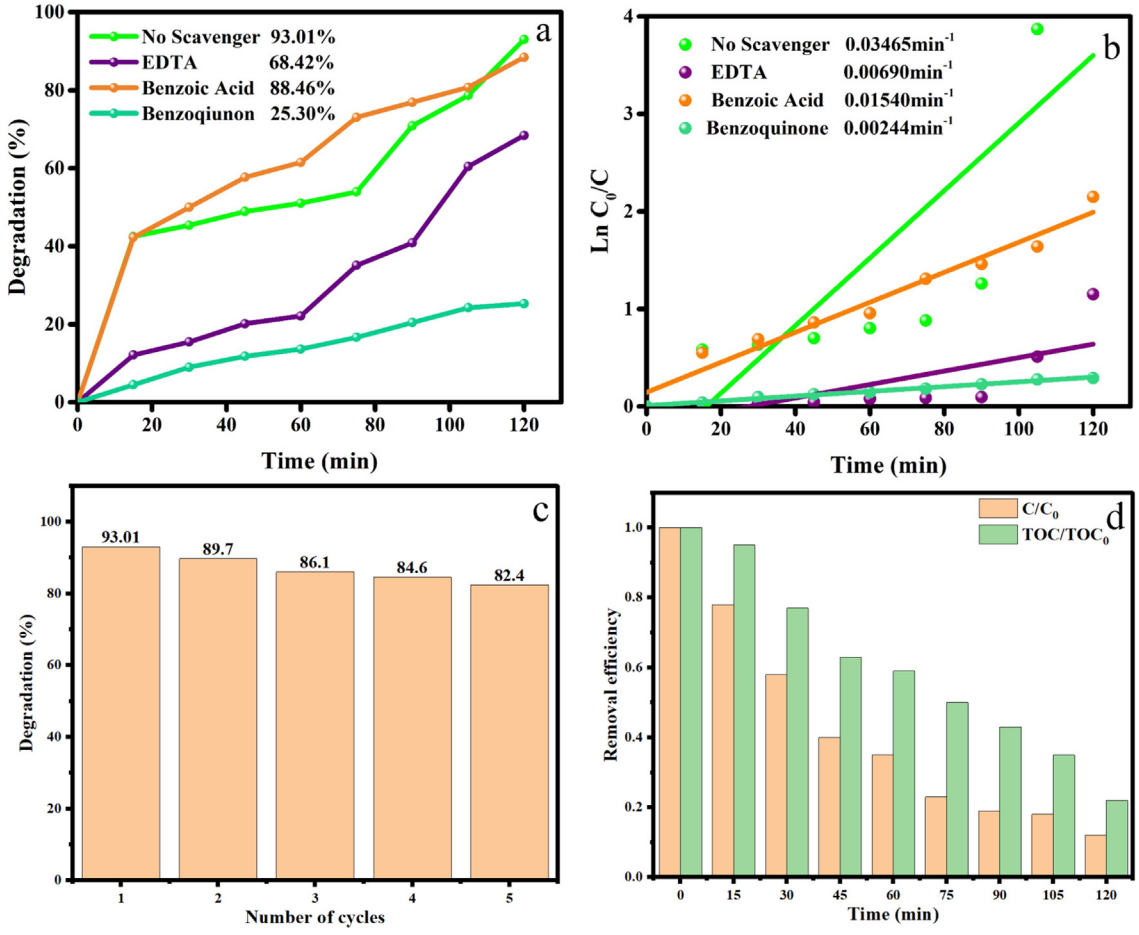

Fig. 11 A) effects of various scavengers on the photocatalytic degradation of ecbt under uv irradiation, b) kinetic linear simulation curves of photocatalytic activity in the presence of scavengers, c) recycle test in the presence of $ho_2Cu_2O_5/Ho_2O_3$ nanocomposites over 10 ppm ECBT, d) TOC removal in the photodegradation of ECBT in the presence $Ho_2Cu_2O_5/Ho_2O_3$ nanocomposites.

Fig. 11c, the degradation efficiency was about 82.4% after five cycles, which decreased by 10.61% compared to the first cycle. The result affirmed that dye decolorization was accomplished by optical technique, in which physical absorption played a minor role.

3.2.3. TOC test

Furthermore, the mineralization of ECBT during the photocatalytic degradation process was also investigated by TOC measurements. As shown in Fig. 11d, the TOC removal ratios over $Ho_2Cu_2O_5/Ho_2O_3$ nanocomposites were gradually promoted with increasing the irradiation time of UV light. After 120 min of photocatalytic reaction, the TOC removal ratio was approximately 78%. That is to say, during the degradation process, most of the dye molecules could be mineralized over the $Ho_2Cu_2O_5/Ho_2O_3$ photocatalyst under UV light illumination (Chen et al., 2021; Ren et al., 2020).

3.2.4. Stability

Fig. 12a depicts the XRD pattern of $Ho_2Cu_2O_5/Ho_2O_3$ nanocomposites after five cycle's degradation. As can be seen, all diffraction peaks well-matched to $Ho_2Cu_2O_5$ (JCDPS No. 00–033-0458) and Ho_2O_3 (JCDPS No. 01–074-1984) with orthorhombic structure. The result showed that the photocatalytic reaction did not change the crystal structure of nanocomposites. FESEM images of $Ho_2Cu_2O_5/Ho_2O_3$ nanocomposites after five cycle's degradation shows the approximately similar morphology of before degradation (Fig. 12a and 12b). These result confirm the high stability of $Ho_2Cu_2O_5/Ho_2O_3$ nanocomposites.

3.2.5. Comparison study

For in-depth investigation, the results obtained from the photocatalytic performance of the as-obtained $Ho_2Cu_2O_5/Ho_2O_3$ nanocomposites were compared with previously reported

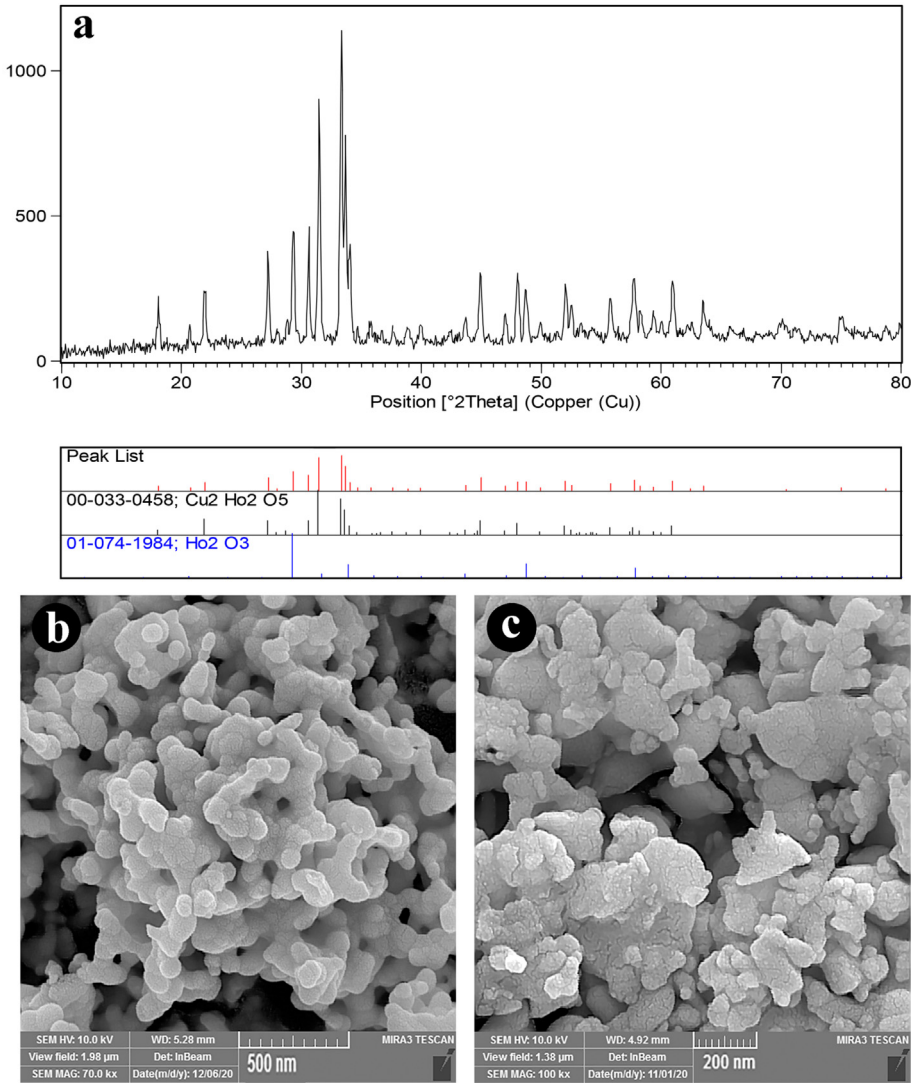

Fig. 12 A) xrd pattern, (b and c) fesem images of $ho_2Cu_2O_5/Ho_2O_3$ nanocomposites after five cycle's photodegradation.

Table 1 Comparison of photocatalytic performance of some photocatalyst and current $Ho_2Cu_2O_5/Ho_2O_3$ nanocomposites.

Sample	Dye	Efficiency (%)	Time (min)	References
Er-doped CuO	Reactive Black 5	98.0	90	(Shaghaghi et al., 2020)
Eu-doped ZnO	Eriochrome Black T	99.0	240	(Franco et al., 2020)
$HoVO_4$	Methyl Violet	67.6	90	(Khorasanizadeh et al., 2019)
(Er, Yb) co-doped ZnO	Methyl Orange	99.0	90	(Ahmad, 2019)
ZnO/CuO	Rhodamine B	95.0	100	(Kumari et al., 2020)
g-C3N4/Ce_2O_3/CuO	Methylene Blue	90.3	150	(Vignesh et al., 2022)
$La_2Cu_2O_5$	Acid Black	80.1	120	(Tabatabaeinejad et al., 2022)
$Dy_2Cu_2O_5$	Phenol Red	96.4	120	(Tabatabaeinejad, Amiri, et al., 2021)
La_2CuO_4-ZnO	Malachite Green	91.0	120	(Yulizar et al., 2020)
$Lu_2Cu_2O_5/Lu_2O_3$	Thymol Blue	98.5	120	(Tabatabaeinejad, Zinatloo-Ajabshir, et al., 2021)
ZnO/La_2O_3/NiO	Methylene Blue	98.0	150	(Shubha et al., 2022)
CuO	Methylene Blue	85.0	50	(Muthuvel et al., 2020)
Pt/PtO Nanodots onLa_2O_3	Methyl Orange	98.0	120	(Zhao et al., 2020)
$Sm_2Ti_2O_7$	Rhodamine B	94.0	80	(Kaviyarasu et al., 2020)
$La_2Sn_2O_7$	Methyl Orange	98.0	50	(Zeng et al., 2007)
$La_2Ti_2O_7$	Reactive Red 22	99.0	180	(Hou & Ku, 2011)
$Ce_2Sn_2O_7$	Methylene Blue	80.0	60	(Jayaraman et al., 2019)
$Ho_2Cu_2O_5/Ho_2O_3$	Eriochrome Black T	93.01	120	This work

papers on the degradation of water pollutants (Table 1). As can be seen, $Ho_2Cu_2O_5/Ho_2O_3$ nanocomposites can compete with other similar structure and can be a great photocatalyst for water purification process.

4. Conclusion

In this work, $Ho_2Cu_2O_5/Ho_2O_3$ photocatalyst was successfully prepared via the fast and simple ultrasonic-assisted method. The sufficient optical bandgaps of $Ho_2Cu_2O_5/Ho_2O_3$ photocatalyst lead to the degradation of various organic pollutants under UV light. The highest photocatalytic efficiency was obtained against Eriochrome black T (ECBT), and 93% of ECBT was degraded after 120 min. Further investigation revealed that the highest photocatalytic activity was achieved under the optimum condition of 0.03 g of $Ho_2Cu_2O_5/Ho_2O_3$ and 10 ppm of ECBT. The rate of the pseudo-first-order reaction was calculated at 0.03465 min^{-1} via photodegradation kinetic investigation. It was suggested that the photocatalytic degradation of ECBT was carried out using $^{\bullet}O_2^-$ radicals via applying benzoquinone as an $\bullet O_2^-$ scavenging.

CRediT authorship contribution statement

Seyed Milad Tabatabaeinejad: Formal analysis, Investigation, Software, Methodology, Formal analysis. **Hossein Safardoust-Hojaghan:** Writing – original draft, Investigation, Software. **Mojgan Ghanbari:** Writing – review & editing, Investigation, Software. **Hasan Sh. Majdi:** Software, Writing – review & editing. **Shuaib M. Abdulnabi:** Software, Visualization. **Furqan S. Hashim:** Software, Validation. **Anmar Ghanim Taki:** Software. **Masoud Salavati-Niasari:** Formal analysis, Writing – review & editing, Conceptualization, Supervision, Project administration, Visualization, Writing – original draft, Writing – review & editing, Data curation, Validation, Resources.

Acknowledgments

Authors are thankful to the council of Iran National Science Foundation (INSF, 97017837) and University of Kashan for supporting this work by Grant No (159271/SMT4).

References

Abdolmohammad-Zadeh, H., Zamani-Kalajahi, M., 2020. In situ generation of H2O2 by a layered double hydroxide as a visible light nano-photocatalyst: Application to bisphenol A quantification. Microchem. J. 158,. https://doi.org/10.1016/j.microc.2020.105303 105303.

Abdtawfeeq, T.H., Farhan, Z.A., Al-Majdi, K., Jawad, M.A., Zabibah, R.S., Riadi, Y., Hadrawi, S.K., AL-Alwany, A., Shams, M.A., 2022. Ultrasound-Assisted and One-Pot Synthesis of New Fe3O4/Mo-MOF Magnetic Nano Polymer as a Strong Antimicrobial Agent and Efficient Nanocatalyst in the Multicomponent Synthesis of Novel Pyrano [2, 3-d] pyrimidines Derivatives. J. Inorg. Organomet. Polym Mater. 1–12. https://doi.org/10.1007/s10904-022-02514-7.

Ahmad, I., 2019. Inexpensive and quick photocatalytic activity of rare earth (Er, Yb) co-doped ZnO nanoparticles for degradation of methyl orange dye. Sep. Purif. Technol. 227,. https://doi.org/10.1016/j.seppur.2019.115726 115726.

Al Alwany, A.A., 2022. Arrhythmia related to hypertensive left ventricular hypertrophy in Iraqi patients: frequency and outcome. J. Med. Life 15 (9), 1115. https://doi.org/10.25122/jml-2022-0214.

Bobinov, V., Goroshchenko, S., Rozhchenko, L., Samochernykh, K., Petrov, A., 2021. Historical aspects of microsurgical treatment of brain aneurysms. History of Medicine 7 (2), 179–188. https://doi.org/10.17720/2409-5834.v7.2.2021.08h.

Chen, Y., Wang, Y., Fang, J., Dai, B., Kou, J., Lu, C., Zhao, Y., 2021. Design of a ZnO/Poly(vinylidene fluoride) inverse opal film for photon localization-assisted full solar spectrum photocatalysis. Chin. J. Catal. 42 (1), 184–192. https://doi.org/10.1016/S1872-2067(20)63588-4.

Chen, Y., Cheng, M., Lai, C., Wei, Z., Zhang, G., Li, L., Tang, C., Du, L., Wang, G., Liu, H., 2023. The Collision between g-C3N4 and QDs in the Fields of Energy and Environment: Synergistic Effects for Efficient Photocatalysis. Small 2205902.

Deng, Y., Feng, C., Tang, L., Zeng, G., Chen, Z., & Zhang, M. (2019). Chapter 5 - Nanohybrid Photocatalysts for Heavy Metal Pollutant Control. In L. Tang, Y. Deng, J. Wang, J. Wang, & G. Zeng (Eds.), Nanohybrid and Nanoporous Materials for Aquatic Pollution Control (pp. 125-153). Elsevier. DOI: 10.1016/B978-0-12-814154-0.00005-0.

Duan, Y., Ma, J., Dai, J., Qiang, L., Xue, J., 2021. Morphology engineering of ZnO nanostructures for enhanced photocatalytic

efficiency of In(OH)3/ZnO nanocomposite. Appl. Surf. Sci. 535,. https://doi.org/10.1016/j.apsusc.2020.147657 147657.

Franco, P., Sacco, O., De Marco, I., Sannino, D., Vaiano, V., 2020. Photocatalytic Degradation of Eriochrome Black-T Azo Dye Using Eu-Doped ZnO Prepared by Supercritical Antisolvent Precipitation Route: A Preliminary Investigation. Top. Catal. 63 (11), 1193–1205. https://doi.org/10.1007/s11244-020-01279-y.

Fu, W., Yi, J., Cheng, M., Liu, Y., Zhang, G., Li, L., Du, L., Li, B., Wang, G., Yang, X., 2022. When bimetallic oxides and their complexes meet Fenton-like process. J. Hazard. Mater. 424,. https://doi.org/10.1016/j.jhazmat.2021.127419 127419.

Geng, N., Chen, W., Xu, H., Ding, M., Liu, Z., Shen, Z., 2019. A sono-photocatalyst for humic acid removal from water: Operational parameters, kinetics and mechanism. Ultrason. Sonochem. 57, 242–252. https://doi.org/10.1016/j.ultsonch.2019.03.022.

Gondo, H.K., 2022. "Effect of Isotiocyanate Therapy On Trophoblast Cell Culture Hyperglycemia Atmosphere In Apoptosis, Caspase-3, NO. VEGF. History of Medicine 8 (1), 62–67. https://doi.org/10.17720/2409-5834.v8.1.2022.008.

Guo, R., You, J., Han, F., Li, C., Zheng, G., Xiao, W., Liu, X., 2017. Controlled synthesis, formation mechanism, and carbon oxidation properties of Ho2Cu2O5 nanoplates prepared with a coordination-complex method. Appl. Surf. Sci. 396, 1076–1084.

Hou, W.-M., Ku, Y., 2011. Synthesis and characterization of La2Ti2O7 employed for photocatalytic degradation of reactive red 22 dyestuff in aqueous solution. J. Alloy. Compd. 509 (19), 5913–5918.

Hujjatul Islam, M., Paul, M.T.Y., Burheim, O.S., Pollet, B.G., 2019. Recent developments in the sonoelectrochemical synthesis of nanomaterials. Ultrason. Sonochem. 59,. https://doi.org/10.1016/j.ultsonch.2019.104711 104711.

Islam, M.R., Saiduzzaman, M., Nishat, S.S., Kabir, A., Farhad, S.F. U., 2021. Synthesis, characterization and visible light-responsive photocatalysis properties of Ce doped CuO nanoparticles: A combined experimental and DFT + U study. Colloids Surf A Physicochem Eng Asp 617,. https://doi.org/10.1016/j.colsurfa.2021.126386 126386.

Jayaraman, V., Palanivel, B., Ayappan, C., Chellamuthu, M., Mani, A., 2019. CdZnS solid solution supported Ce2Sn2O7 pyrochlore photocatalyst that proves to be an efficient candidate towards the removal of organic pollutants. Sep. Purif. Technol. 224, 405–420.

Kannan, K., Radhika, D., Nesaraj, A.S., Kumar Sadasivuni, K., Reddy, K.R., Kasai, D., Raghu, A.V., 2020. Photocatalytic, antibacterial and electrochemical properties of novel rare earth metal oxides-based nanohybrids. Materials Science for Energy Technologies 3, 853–861. https://doi.org/10.1016/j.mset.2020.10.008.

Kar, P., Shukla, K., Jain, P., Sathiyan, G., Gupta, R.K., 2021. Semiconductor based photocatalysts for detoxification of emerging pharmaceutical pollutants from aquatic systems: A critical review. Nano Materials Science 3 (1), 25–46. https://doi.org/10.1016/j.nanoms.2020.11.001.

Kaviyarasu, K., Magdalane, C.M., Jayakumar, D., Samson, Y., Bashir, A., Maaza, M., Letsholathebe, D., Mahmoud, A.H., Kennedy, J., 2020. High performance of pyrochlore like Sm2Ti2O7 heterojunction photocatalyst for efficient degradation of rhodamine-B dye with waste water under visible light irradiation. Journal of King Saud University-Science 32 (2), 1516–1522.

Khataee, A., Rahim Pouran, S., & Hassani, A. (2020). Editorial note-Special Issue on "Ultrasonic Nanotechnology: New insights into industrial and environmental Applications". *Ultrasonics Sonochemistry*, *65*, 104878. DOI: 10.1016/j.ultsonch.2019.104878.

Khorasanizadeh, M.H., Monsef, R., Amiri, O., Amiri, M., Salavati-Niasari, M., 2019. Sonochemical-assisted route for synthesis of spherical shaped holmium vanadate nanocatalyst for polluted waste water treatment. Ultrason. Sonochem. 58, 104686.

Kumari, V., Yadav, S., Jindal, J., Sharma, S., Kumari, K., Kumar, N., 2020. Synthesis and characterization of heterogeneous ZnO/CuO hierarchical nanostructures for photocatalytic degradation of organic pollutant. Adv. Powder Technol. 31 (7), 2658–2668. https://doi.org/10.1016/j.apt.2020.04.033.

Liu, Y., Cheng, H., Cheng, M., Liu, Z., Huang, D., Zhang, G., Shao, B., Liang, Q., Luo, S., Wu, T., Xiao, S., 2021a. The application of Zeolitic imidazolate frameworks (ZIFs) and their derivatives based materials for photocatalytic hydrogen evolution and pollutants treatment. Chem. Eng. J. 417,. https://doi.org/10.1016/j.cej.2020.127914 127914.

Liu, H., Cheng, M., Liu, Y., Wang, J., Zhang, G., Li, L., Du, L., Wang, G., Yang, S., Wang, X., 2022a. Single atoms meet metal–organic frameworks: collaborative efforts for efficient photocatalysis. Energ. Environ. Sci. 15 (9), 3722–3749.

Liu, Z., Hadi, M.A., Aljuboory, D.S., Ali, F.A., Jawad, M.A., Ameen, A.-A., Hadrawi, S.K., Mundher, T., Riadi, Y., Amer, R.F., 2022b. High efficiency of Ag0 decorated Cu2MoO4 nanoparticles for heterogeneous photocatalytic activation, bactericidal system, and detection of glucose from blood sample. J. Photochem. Photobiol. B Biol. 236,. https://doi.org/10.1016/j.jphotobiol.2022.112571 112571.

Liu, Y., Tang, C., Cheng, M., Chen, M., Chen, S., Lei, L., Chen, Y., Yi, H., Fu, Y., Li, L., 2021b. Polyoxometalate@Metal–Organic Framework Composites as Effective Photocatalysts. ACS Catal. 11 (21), 13374–13396. https://doi.org/10.1021/acscatal.1c03866.

Moghanlou, A.O., Sadr, M.H., Bezaatpour, A., Salimi, F., Yosefi, M., 2021. RGO/Cu2O-CuO nanocomposite as a visible-light assisted photocatalyst for reduction of organic nitro groups to amines. Mol. Catal. 516,. https://doi.org/10.1016/j.mcat.2021.111997 111997.

Mohd Razali, N.A., Wan Salleh, W.N., Aziz, F., Jye, L.W., Yusof, N., Ismail, A.F., 2021. Review on tungsten trioxide as a photocatalysts for degradation of recalcitrant pollutants. J. Clean. Prod. 309,. https://doi.org/10.1016/j.jclepro.2021.127438 127438.

Mosleh, S., Rahimi, M.R., Ghaedi, M., Dashtian, K., Hajati, S., 2018. Sonochemical-assisted synthesis of CuO/Cu2O/Cu nanoparticles as efficient photocatalyst for simultaneous degradation of pollutant dyes in rotating packed bed reactor: LED illumination and central composite design optimization. Ultrason. Sonochem. 40, 601–610. https://doi.org/10.1016/j.ultsonch.2017.08.007.

Muthuvel, A., Jothibas, M., Manoharan, C., 2020. Synthesis of copper oxide nanoparticles by chemical and biogenic methods: photocatalytic degradation and in vitro antioxidant activity. Nanotechnology for Environmental Engineering 5, 1–19.

Parvizi, E., Tayebee, R., Koushki, E., Abdizadeh, M.F., Maleki, B., Audebert, P., Galmiche, L., 2019. Photocatalytic efficacy of supported tetrazine on MgZnO nanoparticles for the heterogeneous photodegradation of methylene blue and ciprofloxacin. RSC Adv. 9 (41), 23818–23831.

Patra Shahi, M., Kumari, P., Mahobiya, D., Kumar Shahi, S., 2021. Chapter 4 - Nano-bioremediation of environmental contaminants: applications, challenges, and future prospects. In: Kumar, V., Saxena, G., Shah, M.P. (Eds.), Bioremediation for Environmental Sustainability. Elsevier, pp. 83–98. https://doi.org/10.1016/B978-0-12-820318-7.00004-6.

Raizada, P., Sudhaik, A., Patial, S., Hasija, V., Parwaz Khan, A.A., Singh, P., Gautam, S., Kaur, M., Nguyen, V.-H., 2020. Engineering nanostructures of CuO-based photocatalysts for water treatment: Current progress and future challenges. Arab. J. Chem. 13 (11), 8424–8457. https://doi.org/10.1016/j.arabjc.2020.06.031.

Rathi, B.S., Kumar, P.S., Vo, D.-V.-N., 2021. Critical review on hazardous pollutants in water environment: Occurrence, monitoring, fate, removal technologies and risk assessment. Sci. Total Environ. 797,. https://doi.org/10.1016/j.scitotenv.2021.149134 149134.

Ren, Z., Liu, X., Zhuge, Z., Gong, Y., Sun, C.Q., 2020. MoSe2/ZnO/ZnSe hybrids for efficient Cr(VI) reduction under visible light irradiation. Chin. J. Catal. 41 (1), 180–187. https://doi.org/10.1016/S1872-2067(19)63484-4.

Reza, K.M., Kurny, A.S.W., Gulshan, F., 2017. Parameters affecting the photocatalytic degradation of dyes using TiO2: a review. Appl Water Sci 7 (4), 1569–1578. https://doi.org/10.1007/s13201-015-0367-y.

Sajjadi, M., Ahmadpoor, F., Nasrollahzadeh, M., Ghafuri, H., 2021. Lignin-derived (nano)materials for environmental pollution remediation: Current challenges and future perspectives. Int. J. Biol. Macromol. 178, 394–423. https://doi.org/10.1016/j.ijbiomac.2021.02.165.

Salavati-Niasari, M., Davar, F., Fereshteh, Z., 2009. Synthesis and characterization of ZnO nanocrystals from thermolysis of new precursor. Chem. Eng. J. 146 (3), 498–502. https://doi.org/10.1016/j.cej.2008.09.042.

Salavati-Niasari, M., Hasanalian, J., Najafian, H. 2004. Alumina-supported FeCl3, MnCl2, CoCl2, NiCl2, CuCl2, and ZnCl2 as catalysts for the benzylation of benzene by benzyl chloride; Journal of Molecular Catalysis A: Chemical 209(1-2), 209-214. doi.org/10.1016/j.molcata.2003.08.027.

Salavati-Niasari, M. 2005. Synthesis and characterization of host (nanodimensional pores of zeolite-Y)–guest [unsaturated 16-membered octaaza–macrocycle manganese (II), cobalt (II), nickel (II), copper; Chemistry letters 34(10), 1444-1445. doi.org/10.1246/cl.2005.1444.

Serpone, N., Emeline, A.V., 2012. Semiconductor Photocatalysis — Past, Present, and Future Outlook. The Journal of Physical Chemistry Letters 3 (5), 673–677. https://doi.org/10.1021/jz300071j.

Shabani, A., Nabiyouni, G., Saffari, J., Ghanbari, D., 2016. Photocatalyst Fe3O4/TiO2 nanocomposites: green synthesis and investigation of magnetic nanoparticles coated on cotton. J. Mater. Sci. Mater. Electron. 27 (8), 8661–8669. https://doi.org/10.1007/s10854-016-4887-5.

Shaghaghi, Z., Amani-Ghadim, A.R., Seraji, M., 2020. Structural properties and photocatalytic degradation efficiency of CuO and erbium doped CuO nanostructures prepared by thermal decomposition of some Cu-salophen type complexes as precursors. Mater. Chem. Phys. 243,. https://doi.org/10.1016/j.matchemphys.2020.122635 122635.

Shawky, A., Albukhari, S.M., Tashkandi, N.Y., Zaki, Z.I., 2021. Photoactivity enhancement of La-doped NaTaO3 nanocrystals by CuO decoration toward fast oxidation of ciprofloxacin under visible light. Ceram. Int. 47 (20), 28884–28891. https://doi.org/10.1016/j.ceramint.2021.07.049.

Shi, Y., Ma, J., Chen, Y., Qian, Y., Xu, B., Chu, W., An, D., 2022. Recent progress of silver-containing photocatalysts for water disinfection under visible light irradiation: A review. Sci. Total Environ. 804,. https://doi.org/10.1016/j.scitotenv.2021.150024 150024.

Shubha, J., Sushma, N., Adil, S., Khan, M., Assal, M.E., Hatshan, M. R., Shaik, B., 2022. ZnO/La2O3/NiO based ternary heterostructure nano-photocatalyst: Preparation, characterization and its application for the degradation of methylene blue. Journal of King Saud University-Science 34, (1) 101738.

Sordello, F., Berruti, I., Gionco, C., Paganini, M.C., Calza, P., Minero, C., 2019. Photocatalytic performances of rare earth element-doped zinc oxide toward pollutant abatement in water and wastewater. Appl Catal B 245, 159–166. https://doi.org/10.1016/j.apcatb.2018.12.053.

Sutar, S., Otari, S., Jadhav, J., 2022. Biochar based photocatalyst for degradation of organic aqueous waste: A review. Chemosphere 287,. https://doi.org/10.1016/j.chemosphere.2021.132200 132200.

Tabatabaeinejad, S.M., Amiri, O., Ghanbari, M., Salavati-Niasari, M., 2021a. Dy2Cu2O5 nanostructures: Sonochemical fabrication, characterization, and investigation of photocatalytic ability for elimination of organic contaminants. J. Mol. Liq. 344, 117883.

Tabatabaeinejad, S.M., Zinatloo-Ajabshir, S., Amiri, O., Salavati-Niasari, M., 2021b. Magnetic Lu 2 Cu 2 O 5-based ceramic nanostructured materials fabricated by a simple and green approach for an effective photocatalytic degradation of organic contamination. RSC Adv. 11 (63), 40100–40111.

Tabatabaeinejad, S.M., Ghanbari, M., Najm, Z.M., Abdul-Fattah, M. N., Hameed, N.M., Salavati-Niasari, M., 2022. Facile sonochemical preparation of La2Cu2O5 nanostructures, characterization, the evaluation of performance, mechanism, and kinetics of photocatalytic reactions for the removal of toxic pollutants. J. Mol. Liq. 362, 119718.

Tang, C., Cheng, M., Lai, C., Li, L., Yang, X., Du, L., Zhang, G., Wang, G., Yang, L., 2023. Recent progress in the applications of non-metal modified graphitic carbon nitride in photocatalysis. Coord. Chem. Rev. 474, 214846.

Tayebee, R., Esmaeili, E., Maleki, B., Khoshniat, A., Chahkandi, M., Mollania, N., 2020. Photodegradation of methylene blue and some emerging pharmaceutical micropollutants with an aqueous suspension of WZnO-NH2@ H3PW12O40 nanocomposite. J. Mol. Liq. 317, 113928.

Tobaldi, D.M., Lajaunie, L., López Haro, M., Ferreira, R.A.S., Leoni, M., Seabra, M.P., Calvino, J.J., Carlos, L.D., Labrincha, J.A., 2019. Synergy of Neodymium and Copper for Fast and Reversible Visible-light Promoted Photochromism, and Photocatalysis, in Cu/Nd-TiO2 Nanoparticles. ACS Applied Energy Materials 2 (5), 3237–3252. https://doi.org/10.1021/acsaem.9b00084.

Vignesh, S., Suganthi, S., Palanivel, B., Ali, A.M., Shkir, M., Algarni, H., Sreedevi, G., 2022. Design a novel g-C3N4 based Ce2O3/CuO ternary photocatalysts for superior photo-degradation performance of organic mixed pollutants: Insights of Z-scheme charge transfer mechanism. J. Phys. Chem. Solid 162,. https://doi.org/10.1016/j.jpcs.2021.110514 110514.

Wang, J., Su, G., Yan, X., Zhang, W., Jia, J., Yan, B., 2022. Predicting cytotoxicity of binary pollutants towards a human cell panel in environmental water by experimentation and deep learning methods. Chemosphere 287,. https://doi.org/10.1016/j.chemosphere.2021.132324 132324.

Wang, S., Zheng, Y., Cai, E., 2021. Structure and optical characteristics of Fe9TiO10 semiconductor applied as magnetically recyclable photocatalyst. Ceram. Int. 47 (2), 2641–2648. https://doi.org/10.1016/j.ceramint.2020.09.112.

Wei, Y., Li, X., Zhang, Y., Yan, Y., Huo, P., Wang, H., 2021. G-C3N4 quantum dots and Au nano particles co-modified CeO2/Fe3O4 micro-flowers photocatalyst for enhanced CO2 photoreduction. Renew. Energy 179, 756–765. https://doi.org/10.1016/j.renene.2021.07.091.

Wen, J., Ma, C., Huo, P., Liu, X., Wei, M., Liu, Y., Yao, X., Ma, Z., Yan, Y., 2017. Construction of vesicle CdSe nano-semiconductors photocatalysts with improved photocatalytic activity: Enhanced photo induced carriers separation efficiency and mechanism insight. J. Environ. Sci. 60, 98–107. https://doi.org/10.1016/j.jes.2016.12.023.

Xiao, W., Cheng, M., Liu, Y., Wang, J., Zhang, G., Wei, Z., Li, L., Du, L., Wang, G., Liu, H., 2023. Functional Metal/Carbon Composites Derived from Metal-Organic Frameworks: Insight into Structures, Properties, Performances, and Mechanisms. ACS Catal. 13, 1759–1790.

Xie, L., Du, T., Wang, J., Ma, Y., Ni, Y., Liu, Z., Zhang, L., Yang, C., Wang, J., 2021. Recent advances on heterojunction-based photocatalysts for the degradation of persistent organic pollutants. Chem. Eng. J. 426,. https://doi.org/10.1016/j.cej.2021.130617 130617.

Xu, X., Yang, Y., Jin, H., Pang, B., Jiang, C., Shao, D., Shi, J., 2021. Filamentous fungal in situ biosynthesis of heterogeneous Au/Cd0.5Zn0.5S nano-photocatalyst: A macroscopic assembly strategy for preparing composite mycelial pellets with visible light degradation ability. J. Hazard. Mater. 406,. https://doi.org/10.1016/j.jhazmat.2020.124797 124797.

Yousefzadeh, F., Yousif, Q.A., Ghanbari, M., Salavati-Niasari, M., 2022. Fabrication of TlSnI3/C3N4 nanocomposites for enhanced photodegradation of toxic contaminants below visible light and investigation of kinetic and mechanism of photocatalytic reaction. J. Mol. Liq. 118443.

Yulizar, Y., Apriandanu, D.O.B., Ashna, R.I., 2020. La2CuO4-decorated ZnO nanoparticles with improved photocatalytic activity for malachite green degradation. Chem. Phys. Lett. 755, 137749.

Zeng, J., Wang, H., Zhang, Y., Zhu, M.K., Yan, H., 2007. Hydrothermal synthesis and photocatalytic properties of pyrochlore La2Sn2O7 nanocubes. J. Phys. Chem. C 111 (32), 11879–11887.

Zhang, L., Ran, J., Qiao, S.-Z., Jaroniec, M., 2019. Characterization of semiconductor photocatalysts [10.1039/C9CS00172G]. Chem. Soc. Rev. 48 (20), 5184–5206. https://doi.org/10.1039/C9CS00172G.

Zhang, T., Su, J., Guo, L., 2016. Morphology engineering of WO3/BiVO4 heterojunctions for efficient photocatalytic water oxidation [10.1039/C6CE01952H]. CrstEngComm 18 (46), 8961–8970. https://doi.org/10.1039/C6CE01952H.

Zhao, Z., Liu, J., Qin, M., Kou, K., Wu, G., Wu, H., 2020. Effective cocatalyst Pt/PtO nanodots on La2O3 microspheres for degradation of methyl orange. J. Nanosci. Nanotechnol. 20 (5), 3140–3147.